The effect of prior ultrasonic shot peening treatment on the low-temperature plasma nitriding of a metastable β-Ti alloy

Renaud Genin, Luc Pichon, Antoine Guitton, Michel Drouet, Thierry Grosdidier

THE EFFECT OF PRIOR ULTRASONIC SHOT PEENING TREATMENT ON THE LOW-TEMPERATURE PLASMA NITRIDING OF A METASTABLE β-Ti ALLOY

Renaud Génin[1,2,3,*], Luc Pichon[1], Antoine Guitton[2,3], Michel Drouet[1], Thierry Grosdidier[2,3]

1 Institut Pprime, UPR3346, CNRS Université de Poitiers ISAE-ENSMA, Département Physique et Mécanique des Matériaux, SP2MI TSA 41123, 86073 Poitiers Cedex, France
2 Université de Lorraine, CNRS, Arts et Métiers, LEM3, Metz 57070, France
3 LABoratoire D'EXcellence "Design of Alloy Metals for Low-mAss Structures" (LABEX-DAMAS), 7 Rue Félix Savart, 57073, Metz, France

*Corresponding author : renaud.genin@univ-lorraine.fr

Metastable β-Ti alloys have recently gained popularity for the fabrication of medical implants such as prostheses. However, they suffer from poor tribological properties. Surface treatments such as plasma nitriding and ultrasonic shot peening both have been successfully used to this end. The ultrasonic shot peening treatment induces surface nanocrystallization and introduces many structural defects in the surface layers. These defects increase the reactivity of the surface and enhance the diffusion of chemical species, which is beneficial to the nitriding kinetics. In this study, an ultrasonic shot peening treatment was applied to two microstructures, namely equiaxial α + β and metastable β, of the Ti-5553 alloy before nitriding at low temperature. The results show much finer secondary α precipitation for the initial β microstructure subjected to USP and nitrided, the formation of sparsely dispersed equiaxial α grains, and that some of the deformation induced by the USP treatment remains after nitriding.

Keywords: Ti-5553, metastable β-Ti, ultrasonic shot peening, plasma nitriding

1. Introduction

Owing to their low Young's modulus, excellent corrosion resistance, strength to weight ratio, and biocompatibility, metastable β Titanium alloys are now widely used in several industries, including biomedical [1], and aerospace [2]. However, when prostheses are subjected to low strain but very high-cycle fatigue, these types of alloys tend to suffer from poor tribological properties [3], which can lead to the release of potentially harmful metallic ions in the body [1]. Surface hardening treatments have been developed to overcome these shortcomings. These can be split into two main categories : thermochemical and mechanical processes. They consist of introducing a property gradient from the surface towards the bulk of the work piece.

Thermochemical processes have been used to improve the tribological properties of alloys for more than a century. The formation of very hard compounds such as oxides, nitrides, and carbides on the surface as well as the introduction of oxygen, nitrogen, carbon in an interstitial solid solution in the underlying layers ensures significant hardening at the surface and a property gradient through the depth [4]. They typically use immersion in reactive gas or cold plasma combined with thermal activation. The outer compound is often substantially harder than the solid solution. This can lead to a sharp property gradient, which, when subjected to solicitations, can lead to rupture at the interface of the different compounds, the so-called "egg-shell effect" [5]. The parameters of the thermochemical treatments (temperature, duration, mixture of gases, initial microstructure, surface finish, …) can be adjusted to achieve a relatively smooth property gradient and promote adhesion between the layers.

Mechanical treatments rely on strain hardening and compressive residual stresses to achieve local property modifications. Techniques such as shot peening have been commonly used to this end [6, 7]. More recently, the advent of Surface Severe Plastic Deformation (SSPD) processes has offered new opportunities for property modification through mechanical treatments. Indeed, they have been used to refine the grain size down to the nanometer scale [8-10]. Several SSPD processes have been designed specifically to enhance the surface properties of metallic alloys. The most common are Ultrasonic Shot Peening (USP) and Superficial Mechanical Attrition Treatment (SMAT) but several alternative processes have been used to achieve similar results too. Surface nanocrystallization and the introduction of compressive residual stresses under the surface are the most common effects of these processes. Mechanical characterization reveals significant hardening near the surface, enhanced yield strength, fatigue resistance, and wear resistance [9, 10]. In titanium, the nanocrystalline surface layer has demonstrated improved corrosion resistance, and significantly enhanced surface reactivity [7-14].

The diffusion kinetics of chemical species can be greatly improved by the presence of structural defects formed by SSPD. Thus, the nanocrystalline layer formed is susceptible to an enhanced reactivity during subsequent thermochemical treatment. This process has been studied in the case of stainless steels [15], commercially pure titanium, and some α + β Ti alloys [12-14]. The authors report lower required nitriding temperatures and durations, thicker and harder surface compound layers. In the case of titanium alloys, most of the studies were done

on Ti-6Al-4V. The thermal stability of the deformation induced by the SPD treatment in Ti alloys was investigated and complete recrystallization seems to be achieved after annealing 5h at 600°C [13]. Some metastable β-Ti alloys subjected to SSPD processes exhibit non-classical deformation mechanisms, namely kink bands [16, 17]. Studies have shown that in some cases, damage is highly localized in the deformation bands, and have proposed hypotheses to explain the significant grain refinement that occurs inside the bands [18, 19]. The effect of subsequent nitriding has never been tested on β-Ti alloys.

This manuscript presents the first results of an ongoing research in which the USP treatment followed by subsequent low-temperature nitriding was applied to Ti-5Al-5Mo-5V-3Cr (wt. %), a recently developed metastable β-Ti alloy, with two initial microstructures : one 100% β, and the other equiaxial α + β. The microstructure transformations and the chemical composition of the surface layer were studied with X-Ray Diffraction (XRD), Scanning Electron Microscopy (SEM), including Electron Back-Scattering Diffraction (EBSD).

2. Experiments

The Ti-5553 used in this study was provided by Timet Savoie France. Some samples were treated by USP as received (AR) with a α + β equiaxial microstructure. The others were first solution-treated at 925°C for 1h under secondary vacuum and then water-quenched (WQ), which resulted in coarse-grained near 100% β-Ti microstructure. Both types of samples were polished with #1000 grit SiC abrasive paper and then subjected to USP treatment. The treated surface was cleaned with acetone and ethanol before nitriding. AR and WQ samples that were nitrided without USP pre-treatment were polished to a mirror-finish before being inserted in the reactor. The names given to the different samples after each treatment are given in table 1.

Table 1 : Sample names after the different treatments

Initial structure	USP	Nitriding	USP + nitriding
AR	AR-U	AR-N	AR-U-N
WQ	WQ-U	WQ-N	WQ-U-N

The USP treatment was done using balls made of AISI 52100 steel with a 2mm diameter. The vibrating ultrasonic device was set to a frequency of 20kHz with an amplitude of 60µm for 30min. The specifics of the setup were detailed previously in [16]. The nitriding plasma reactor [20] was initially pumped down to 5.10^{-4} µbar and then heated to 550°C while the sample stayed in a cooler zone. Then a 60:40 (vol. %) mixture of N_2:H_2 gas was introduced and regulated at the working pressure of 50 µbar. The plasma was ignited through the application of a Radio Frequency power of 700W, and the sample was introduced in the heated working zone of the reactor. These conditions were maintained for 8h before slowly cooling the samples under vacuum.

X-Ray Diffraction measurements were realized in θ-2θ geometry (Bragg-Brentano) with a LynxEyes linear detector on a Bruker D8 diffractometer equipped with a Cu source. Cross-section analyses were carried out after mechanical-chemical polishing. The back-scattered electronic (BSE) micrographs and chemical composition profiles were obtained by a Zeiss Supra 40 scanning electron microscope equipped with an EDS detector. The EBSD measurements were performed with JEOL F100 SEM equipped with an electron backscattering diffraction detector and Aztec software. The maps issued from the EBSD data were created with ATEX software [21].

3. Results and discussion

3.1. Initial microstructures

Fig. 1 depicts the cross-section SEM micrograph of the initial microstructure of the AR sample. It has an equiaxial α + β microstructure, with globular primary (α_p) grains. Lamellar secondary (α_s) precipitates are distributed within the β grains, and their widths range from 50 to 100nm. The WQ sample (fig. 2) has a near 100% β microstructure. Both were confirmed by XRD measurements (figs. 4 and 5, blue lines). Due to the temperature and duration of the solution treatment, the β grains are several hundred microns in size.

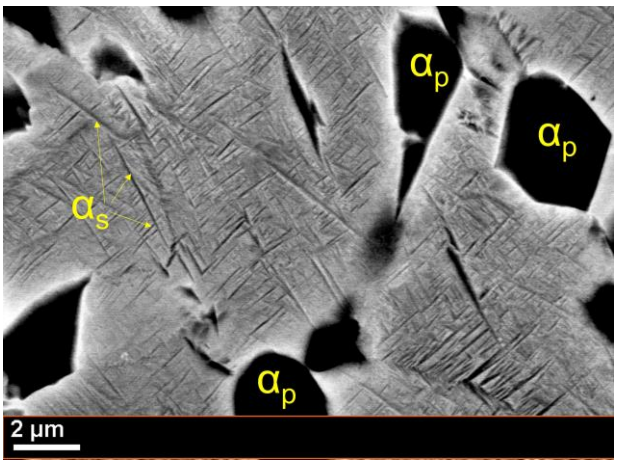

Figure 1. BSE micrograph of the microstructure of the AR sample.

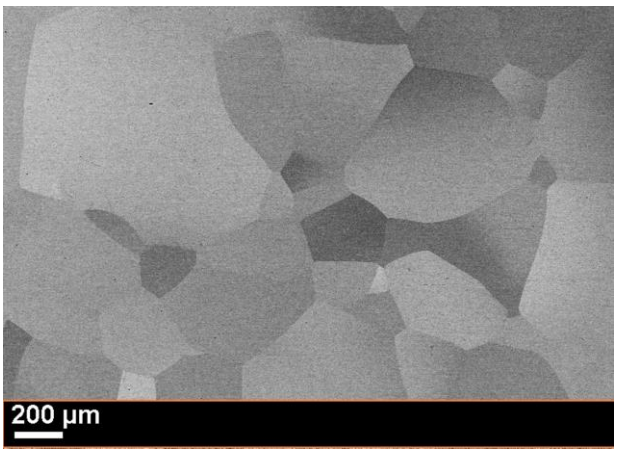

Figure 2. BSE micrograph of the microstructure of the WQ sample.

3.2. Ultrasonic Shot Peening (USP)

Figure 3 shows the band slope map constructed from the EBSD measurements done on the cross-sections of a) the AR-U sample, and b) the WQ-U sample. Non-indexed pixels are displayed in black. The band slope criterion is an indicator of the quality of the EBSD indexation per pixel [22]. The map in fig. 3.a shows good indexation of the primary α grains close to the surface. Comparatively, the β-Ti matrix within ~50 µm of the surface is mostly non-indexed and exhibits a band slope gradient as the depth progresses.

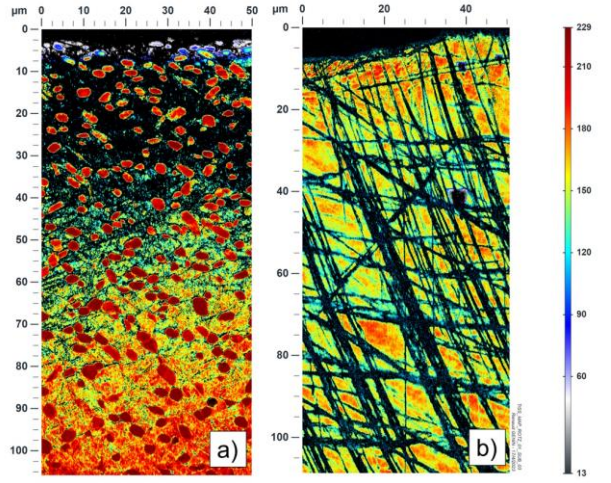

Figure 3. EBSD maps of the cross section of the surface of a) AR + USP sample, and b) WQ + USP sample. The color scale is the band slope. The top surface was the one subjected to USP.

A non-indexed pixel means that the software failed to find a close enough fit for the locally obtained Kikuchi diffraction pattern. This can be caused by several phenomena such as a grain size that is smaller than the step size used for the EBSD measurement, or if the crystallographic lattice is very deformed. Here, the unindexed surface layer and band slope gradient are indicative of the extensive deformation experienced by the top layer. Fig 3.b shows a drastically different deformed state for the β initial structure, with a large number of non-indexed elongated bands of varying thicknesses. Such bands have previously been identified as kink-bands [16, 17]. Considering that these bands are not indexed but the area around is, a significant localization of the deformation within the bands is observed, which according to [18, 19], are prime conditions for grain refinement down to the nanometer scale within the bands.

Figures 4 and 5 present the diffractograms obtained for all the different treatments realized on the AR and WQ initial microstructures, respectively. With respect to the initial samples (blue lines), α and β-Ti peaks of AR-U and WQ-U samples show significant broadening, as well as a slight shift towards the lower angles. Grain refinement and the introduction of residual stresses are known to have a broadening effect as well as reducing the intensity of the diffraction peaks due to the defects present in the crystal lattice [23]. The shift towards the lower angles implies an increase of the interplanar distance for planes parallel to the treated surface that may be related to the introduction of residual stresses by the USP treatment.

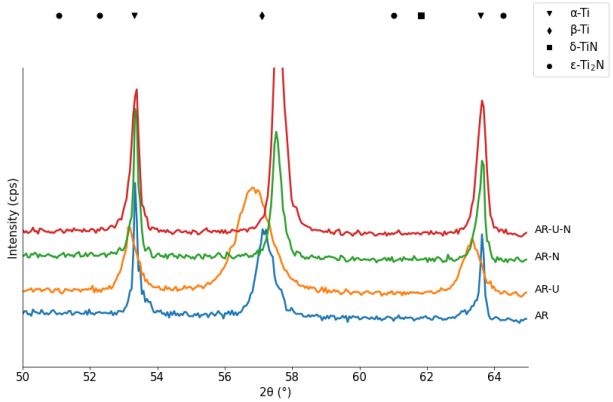

Figure 4. Diffraction patterns for samples : AR, AR-U, AR-N, and AR-U-N

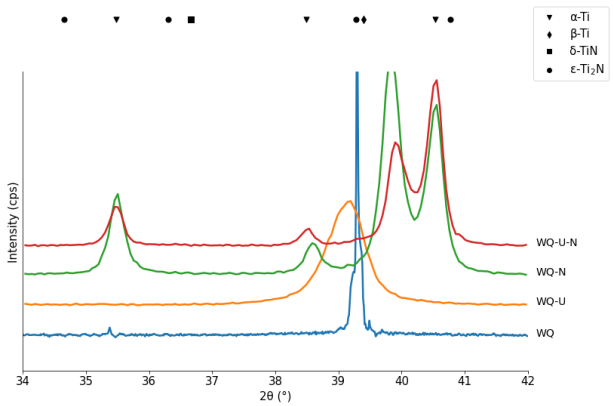

Figure 5. Diffraction patterns for samples : WQ, WQ-U, WQ-N, and WQ-U-N

3.3. *Low-temperature nitriding*

The low-temperature nitriding treatment was carried out on mirror polished AR and WQ samples. In the diffraction patterns of the nitrided samples (figs. 4 and 5, green lines), the α-Ti peaks for the AR-N sample are mostly unchanged, indicating a poor incorporation of Nitrogen in solid solution in α-Ti phase. New distinct peaks corresponding to α-Ti are observed for the WQ-N sample, indicating α precipitation during the nitriding treatment. The β-Ti peaks are shifted towards the higher angles, indicating a decrease of the interplanar distance. This peak shift can be explained by chemical or mechanical effects. During the nitriding treatment, precipitation and coarsening of α-Ti phase occurs, which implies a redistribution of chemical elements by a diffusional process. The β phase is enriched in β stabilizers (Mo, Cr, V) whereas the α stabilizers (Al, N) segregate in α-Ti. The difference in atomic radii relative to Ti atoms induces an increase of the interplanar distance in β-Ti, so this effect is unlikely to be the only one at play here. On the other hand, the observed decreased interplanar distance could be explained by (i) the presence of localized strain at the α/β interfaces caused by the α precipitation, (ii) the formation of tensile strain in the subsurface, or (iii) the relaxation the surface strain that was present in the initial states.

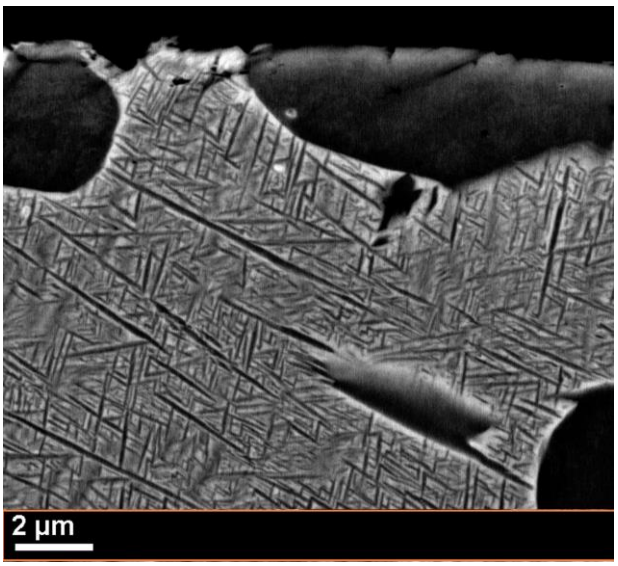

Figure 6. BSE micrograph of the cross-section of the surface microstructure of the AR-N sample. The top surface was the one nitrided.

The cross-sections of the surface microstructure of AR-N and WQ-N samples are shown in figures 6 and 7, respectively. Fig. 6 shows slight coarsening of both the primary α globular grains and the α laths. No change in microstructure can witness the effect of nitriding at this observation scale. The WQ-N sample (fig. 7) shows important precipitation of α laths throughout the β grains. A gradient in α precipitation size is revealed. Finely dispersed laths are present in the closest ~4 µm of the surface while their size is slightly larger underneath. Such fine α precipitation was observed by [24] who showed that sufficiently slow heating (< 20°C/min) led to a modified transformation sequence on heating through the formation of some metastable phases. In the nitriding process performed here however, the rate of heating was very fast. Since this extreme refinement is only found in the surface layer, it is likely to be either the direct effect of minor nitrogen introduction near the surface, or to another precipitation pathway facilitated by the presence of nitrogen.

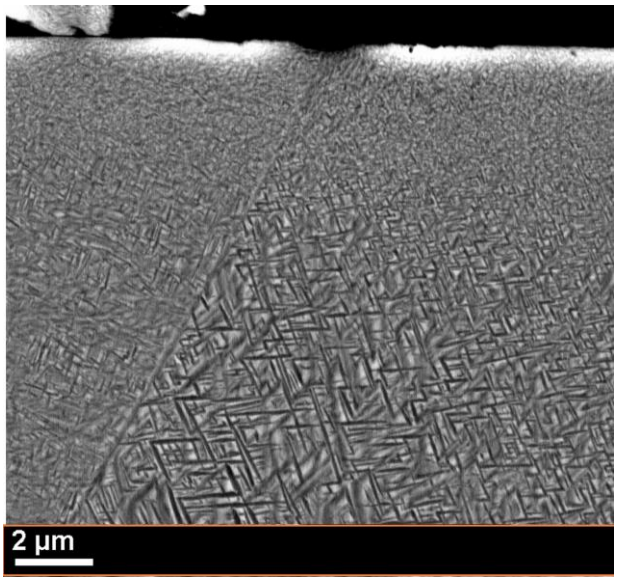

Figure 7. BSE micrograph of the cross-section of the surface microstructure of the WQ-N sample. The top surface was the one nitrided.

3.4. *Ultrasonic Shot Peening followed by low-temperature nitriding*

The red lines in figs. 4 and 5 show the diffractograms obtained for samples AR-U-N and WQ-U-N. Only peaks corresponding to α and β-Ti phases are observed, which indicates that if nitrides were formed, they were present in very small amounts. Compared to AR-N and WQ-N samples, the α and β-Ti peaks obtained are slightly broader, suggesting that some of the deformation induced by the USP treatment is still present after the thermal annealing.

No significant difference could be detected in the SEM BSE cross section micrographs of AR-N (fig. 6) and AR-U-N (not shown). Figure 8 presents the cross-section of the surface microstructure of the WQ-U-N sample. As was the case for the WQ-N sample, precipitation of α laths occurred within the β grains. The plates closer to the surface are also significantly finer. The

major differences attributed to the addition of the USP treatment are revealed by : (i) the much finer precipitation of α laths, (ii) the visible remains of the deformation bands, as well as (iii) the presence of a few globular α grains sparsely dispersed throughout the closest ~30 µm from the surface.

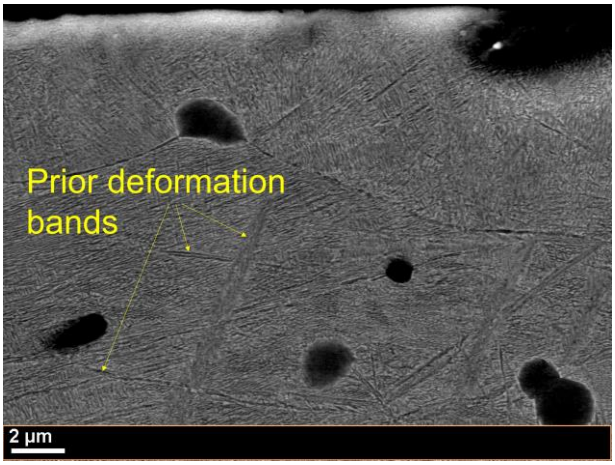

Figure 8. BSE micrograph of the cross-section of the surface microstructure of the WQ-U-N sample. The top surface was the one subjected to USP and then nitrided.

4. Conclusion

Two initial microstructures of metastable Ti-5553 alloy were subjected to USP treatment followed by low-temperature plasma nitriding. The following conclusions could be drawn :

- The USP treatment induces a large number of kink bands in the β phase. XRD results from both α + β and β microstructures confirms significant grain refinement and/or the introduction of residual stresses.
- The low-temperature nitriding treatment causes slight coarsening of α_p and α_s precipitates in the AR-N sample. Fine precipitation of α laths is observed in the WQ-N sample. The precipitation closest to the surface is much finer. No nitride phase could be identified on either sample.
- No significant effect of prior USP treatment on the subsequent nitriding of the AR sample has been observed.
- The USP treatment followed by low-temperature nitriding applied to the 100% β microstructure shows significantly refined α_s precipitation, as well as scarcely dispersed globular α grains close to the treated surface.
- Remains of the deformation induced by the USP treatment are detected after the low-temperature nitriding treatment.

5. Acknowledgements

The authors wish to thank Marc Novelli for performing the USP treatment and his help. This work was supported by the French government through the program “Investissements d’avenir” operated by the French National Research Agency (ANR) and referenced to as ANR-11-LABX-0008-01 (‘LabEx DAMAS’) and ANR-11-LABX-0017-01 (‘LabEx INTERACTIFS’).

6. References

1. L-C. Zhang, L-Y. Chen, *Advanced Engineering Materials* 21 (4) (2019) 1801215
2. R.P. Kolli, A. Devraj, *Metals* 8 (7) (2018) 506.
3. M. Long, H.J. Rack, *Wear* 249 (2001) 158-168.
4. D. Nolan, S.W. Huang, V. Leskovsek, S. Braun, *Surface & Coatings Technology* 200 (2006) 5698-5705.
5. M.I. Bashir, M. Shafiq, M. Naeem, M. Zaka-ul-Islam, J.C. Díaz-Guillén, C.M. Lopez-Badillo, M. Zakaullah, *Surface & Coatings Technology* 327 (2017) 59-65.
6. L. Wagner, *Materials Science & Engineering: A* 263 (2) (1999) 210-216.
7. S. Bagheri, M. Guagliano, *Surface Engineering* 25 (1) (2009) 3-14.
8. K. Edalati et al., *Materials Research Letters* (2022).
9. T. Grosdidier, M. Novelli, *Materials Transactions* 60 (7) (2019) 1344-1355.
10. T.O. Olugbade, J. lu, *Nano Materials Science* 2 (2020) 3-31.
11. R.K. Agrawal, V. Pandey, A. Barhanpurkar-Naik, M.R. Wani, K. Chattopadhyay, V. Singh, *Ultrasonics* 104 (2020) 106110.
12. L. Ge, N. Tian, Z. Lu, C. You, *Applied Surface Science* 286 (2013) 412-416.
13. Q. Yao, J. Sun, G. Zhang, W. Tong, H. Zhang, *Vacuum* 142 (2017) 45-51.
14. J. Sun, Q.T. Yao, Y.H. Zhang, X.D. Du, Y.C. Wu, W.P. Tong, *Surface & Coatings Technology* 309 (2017) 382-389.
15. M. Chemkhi, D. Retraint, A. Roos, C. Demangel, *Surface & Coatings Technology* 325 (2017) 454-461.
16. P. Maurel, L. Weiss, P. Bocher, T. Grosdidier, *Materials Science & Engineering: A* 803 (2021) 140618.
17. Y. Zheng, W. Zeng, Y. Wang, S. Wang, *Materials Science & Engineering: A* 702 (2017) 218-224.
18. A. Zafari, X.S. Wei, W. Xu, K. Xia, *Acta Materialia* 97 (2015) 146-155.

19. K. Li, W. Chen, G.X. Yu, J.Y. Zhang, S.W. Xin, J.X. Liu, X.X. Wang, J. Sun, *Journal of Materials Science & Technology* 120 (2022) 53-64.
20. L. Pichon, T. Girardeau, A. Straboni, M. Drouet, *Journal of Applied Physics* 87 (2) (2000) 925-932.
21. B. Beausir and J.-J. Fundenberger, Analysis Tools for Electron and X-ray diffraction, ATEX-software, www.atex-software.eu, Université de Lorraine - Metz, 2017.
22. A. J. Schwartz, M. Kumar, B. L. Adams, D. P. Field (2014). *Electron backscatter diffraction in materials science*. Springer.
23. N.R. Tao, M.L. Sui, J. Lu, K. Lu, *Nanostructured Materials* 11 (4) (1999) 433-440.
24. T.S. Prithiv, Z. Kloenne, D. Li, R. Shi, Y. Zheng, H.L. Fraser, B. Gault, S. Antonov, *Scripta Materialia* 207 (2022) 114320.